NJC

Cite this: *New J. Chem.*, 2011, **35**, 385–393

www.rsc.org/njc

PAPER

A low band gap donor–acceptor copolymer containing fluorene and benzothiadiazole units: synthesis and photovoltaic properties

Jianing Pei, Shanpeng Wen, Yinhua Zhou, Qingfeng Dong, Zhaoyang Liu, Jibo Zhang and Wenjing Tian*

Received (in Montpellier, France) 19th May 2010, Accepted 5th July 2010
DOI: 10.1039/c0nj00378f

A new low band gap copolymer containing dialkylfluorene and 4,7-dithienyl-2,1,3-benzothiadiazole (TBT), poly(fluorenevinylene-alt-4,7-dithienyl-2,1,3-benzothiadiazole) (PF-TBT) was synthesized by Heck cross-coupling polymerization. The copolymer is soluble in common organic solvents such as chloroform, tetrahydrofuran and chlorobenzene. The TGA result indicated that the copolymer possesses good thermal stability. The absorption, electrochemical and photovoltaic properties of PF-TBT were investigated and compared with those of poly(fluorenevinylene-alt-4,7-diphenyl-2,1,3-benzothiadiazole) (PF-DBT) whose structure is similar to PF-TBT. The copolymer exhibited a broad absorption band with an absorption edge close to 700 nm and an optical band gap of 1.82 eV. Cyclic voltammetry studies indicated that the relatively low HOMO energy level assured a higher open circuit voltage (V_{oc}) when PF-TBT is used as the donor material in a photovoltaic cell. The bulk heterojunction (BHJ) solar cell using PF-TBT as the donor and [6,6]-phenyl C61-butyric acid methyl ester (PCBM) as the acceptor with the structure of ITO/PEDOT : PSS/copolymer : PCBM/LiF/Al, exhibited a V_{oc} of 0.86 V, short-circuit current density (J_{sc}) of 3.97 mA cm^{-2}, fill factor (FF) of 0.35, and a power conversion efficiency (PCE) of 1.18% under one sun of AM 1.5 solar simulator illumination (100 mW cm^{-2}).

Introduction

Polymer solar cells have great potential as candidates for future energy due to low cost, flexibility and large-area fabrication.[1–3] During the past few decades, bulk heterojunction (BHJ) solar cells consisting of a polymer : fullerene blend film as the active layer have been one of the most successful types of polymer solar cells.[4] Up to now, significant effort has been made to synthesise new materials[5–7] and to optimize device structures[8–10] to enhance the efficiency of the polymer solar cells. In order to further improve the efficiency of BHJ solar cells, researchers have paid more attention to the synthesis of novel polymers with a suitable band gap to match solar irradiation,[11–13] a suitable energy level for a high open-circuit voltage (V_{oc}),[14] a high charge carrier mobility[15] and good film forming ability.[16]

To expand the spectral absorption of polymers, one promising method is to introduce an electron-donating unit and an electron-withdrawing unit into the polymer main chain to achieve the alternative donor–acceptor (D–A) copolymers.[17–19] The state of internal charge transfer (ICT) transition from donor to acceptor inside the copolymer absorbs photons with long wavelengths which could extend the absorption and decrease the band gap of the copolymer. Furthermore, the physical properties of the copolymers could be tuned flexibly by changing the donor or acceptor units and the linking bridge between the donor and the acceptor. As usual, thiophene, pyrrole,[20] fluorene and carbazole[21,22] are widely used as electron-donating units, whereas quinoline,[23] quinoxaline,[24] and pyridazine[25] are employed as electron-withdrawing units, and the electron-donating unit and electron-withdrawing unit were connected through a single bond inside the copolymer.

Polyfluorene (PF) and its derivatives are a new class of organic semiconductors due to their unique electro-optical properties, such as high charge carrier mobility and good processability.[26,27] However, the optical band gap of poly(9,9-dialkylfluorene) is *ca.* 3.0 eV,[28] which is too high for efficient sunlight harvesting because the maximum photon flux of sunlight is around 1.7 eV. In order to narrow the band gap of the polymers containing PF for optimal sunlight collection, researchers incorporated an electron-withdrawing unit into the PF main chain to form a D–A alternating arrangement.[29] Previously, we reported a new narrower optical band gap PF-based copolymer,[30] poly(fluorenevinylene-alt-4,7-diphenyl-2,1,3-benzothiadiazole) (PF-DBT; the band

---

State Key Laboratory of Supramolecular Structure and Materials, Jilin University, 2699 Qianjin Avenue, Changchun 130012, P. R. China. E-mail: wjtian@jlu.edu.cn; Fax: + 86431 85193421; Tel: + 86431 85155359

gap of PF-DBT is 2.40 eV, and that of PF is 3.0 eV),[28] which is synthesized by using a phenyl unit as a conjugated bridge between the electron-donating fluorene unit and electron-accepting 2,1,3-benzothiadiazole unit.

To further lower the band gap of PF-based copolymer for efficient sunlight harvesting, here we used a thiophene unit to replace the phenyl unit between the electron-donating fluorene unit and electron-withdrawing 2,1,3-benzothiadiazole unit to synthesize a low band gap D–A copolymer poly(fluorenevinylene-alt-4,7-dithienyl-2,1,3-benzothiadiazole) (PF-TBT). Thiophene was used because it has been shown to have excellent optical and hole-transporting properties as well as an exceptional electron-donating ability and chemical stability in BHJ solar cells.[28] Compared with the previous copolymer **PF-DBT**, **PF-TBT** exhibited a broader absorption band with an absorption edge close to 700 nm and the lower optical band gap (1.82 eV). The BHJ solar cell was fabricated using PF-TBT as the donor and PCBM as the acceptor. The solar cell with a structure of ITO/PEDOT : PSS/copolymer : PCBM/LiF/Al exhibited an open circuit voltage (V_{oc}) of 0.86 V, short-circuit current density (J_{sc}) of 3.97 mA cm^{-2}, fill factor (FF) of 0.35, and a PCE of 1.18% under one sun of AM 1.5 solar simulator illumination (100 mW cm^{-2}).

Experimental section

Materials

All starting materials were purchased from either Acros or Aldrich Chemical Co. and used without further purification, unless otherwise noted. In synthetic preparations, diethyl ether and THF were dried by distillation from sodium/benzophenone under nitrogen. Similarly, DMF and dichloromethane were distilled from CaH_2 under nitrogen. 9,9-Di-*n*-octylfluorene,[31] 2,7-dibromo-9,9-di-*n*-octylfluorene and 4,7-dibromo-2,1,3-benzothiadiazole[32] were prepared according to known literature procedures.

Synthesis

Monomers synthesis

*4,7-Di-2-thienyl-2,1,3-benzothiadiazole (***5***).* To a solution of 4,7-dibromo-2,1,3-benzothiadiazole (**4**) (2.0 g, 6.8 mmol) and tributyl(2-thienyl) stannane (6.1 g, 16.4 mmol) in THF (50 ml), $PdCl_2(PPh_3)_2$ (97 mg, 2 mol%) was added. The mixture was refluxed in a nitrogen atmosphere for 3 h. After the removal of the solvent at a reduced pressure, the residue was purified by column chromatography on silica gel (eluent CH_2Cl_2–hexane, 1 : 1). Recrystallization from ethanol gave the title compound (1.8 g, 80%) as red needles.

^1H NMR (500 MHz, $CDCl_3$): δ 8.11 (d, J = 8.5 Hz, 2H), 7.87 (s, 2H), 7.46 (d, J = 5.0 Hz, 2H), 7.21 (m, 2H). Anal. calcd for $C_{14}H_8N_2S_3$: C, 55.97, H, 2.68, N, 9.32, S, 32.02. Found: C, 56.24; H, 2.92; N, 9.58; S, 32.35.

*4,7-Bis(5-bromo-2-thienyl)-2,1,3-benzothiadiazole (***M-1***).* To a mixture of chloroform (50 mL) and acetic acid (50 mL), **5** (2.0 g, 6.67 mmol) was added in a nitrogen flow. After the solid dissolved completely, *N*-bromosuccinimide (NBS, 2.5 g, 14.01 mmol) was added in one portion. The reaction mixture was stirred at room temperature overnight, and the dark red precipitate formed was filtered off and recrystallized from DMF to give the title compound (1.1 g, 36.3%) as shiny red solid.

^1H NMR (500 MHz, $CDCl_3$): δ 7.81 (d, J = 3.5 Hz, 2H), 7.79 (s, 2H), 7.15 (d, J = 4.0 Hz, 2H). Anal. calcd for $C_{14}H_6N_2S_3Br_2$: C, 36.70; H, 1.32; N, 6.11; S, 20.99. Found: C, 36.98; H, 1.61; N, 6.32; S, 21.52.

*2,7-Diformyl-9,9-di-n-octylfluorene (***3***).* Into a solution of 2,7-dibromo-9,9-di-*n*-octylfluorene (**2**) (6.00 g, 11.0 mmol) in anhydrous THF (100 mL) was added *n*-BuLi (2.5 M in hexane, 9.60 mL, 24.0 mmol) dropwise at −78 °C. After the solution had been stirred for 1 h, anhydrous DMF (2.2 mL, 28.4 mmol) was added dropwise. The resulting mixture was stirred at −78 °C for 30 min and 16 h at room temperature, and then poured into water (400 mL). The mixture was extracted with dichloromethane (3 × 100 mL). The organic extracts were washed with brine, dried with anhydrous $MgSO_4$, and concentrated. The product was purified on a silica gel column with petroleum ether/dichloromethane as the eluent to give pale yellowish green solid in a yield of 69% (3.40 g).

^1H NMR (500 MHz, $CDCl_3$): δ 10.10 (s, 2 H), 7.90–7.94 (m, 6 H), 2.06–2.10 (m, 4 H), 0.91–1.29 (m, 20 H), 0.80 (t, J = 6.9 Hz, 6 H), 0.45–0.61 (m, 4 H). Anal. calcd for $C_{31}H_{42}O_2$: C, 83.36; H, 9.48. Found: C, 83.10; H, 9.16.

*2,7-Diethenyl-9,9-di-n-octylfluorene (***M-2***).* To a solution of 2,7-diformyl-9,9-di-*n*-octylfluorene (**3**) (1.5 g, 3.36 mmol) and triphenylmethylphosphonium bromide (2.93 g, 8.07 mmol) in degassed anhydrous THF (40 mL) was added potassium *tert*-butoxide (1.0 M solution in THF, 9.5 mL, 9.50 mmol) dropwise at 0 °C. The resulting mixture was stirred for 8 h at room temperature and then poured into 150 mL water. The mixture was extracted with petroleum ether (3 × 100 mL). The organic extracts were washed with brine, dried with anhydrous $MgSO_4$, and concentrated. The product was purified on silica gel column with petroleum ether as eluent to afford 1.16 g (78%) product as a colorless oil.

^1H NMR (500 MHz, $CDCl_3$): δ 7.62 (d, J = 8.0 Hz, 2 H), 7.34–7.40 (m, 4 H), 6.80 (dd, J_1 = 11.0 Hz, J_2 = 6.5 Hz, 2 H), 5.80 (d, J = 17.5 Hz, 2 H), 5.25 (d, J = 11.0 Hz, 2 H), 1.93–1.97 (m, 4 H), 1.01–1.30 (m, 20 H), 0.81 (t, J = 7.0 Hz, 6 H), 0.58–0.67 (m, 4 H). Anal. calcd for $C_{33}H_{46}$: C, 89.53; H, 10.47. Found: C, 89.27; H, 10.65.

Polymer synthesis

A flask was charged with a mixture of M-1 (0.174 g, 0.393 mmol), M-2 (0.18 g, 0.393 mmol), $Pd(OAc)_2$ (0.0045 g, 0.035 mmol), P(*o*-tolyl)$_3$ (0.037 g, 0.195 mmol), DMF (8 mL), and triethylamine (2 mL). The flask was degassed and purged with N_2. The mixture was heated at 90 °C for 24 h under nitrogen atmosphere. The polymer was precipitated into 200 mL of methanol, and filtered through a Soxhlet thimble, which was then subjected to Soxhlet extraction with methanol, hexane, acetone, and chloroform. The fraction from chloroform was concentrated under reduced pressure and precipitated into methanol (200 mL), and collected by filtration. The final product was dried under vacuum overnight to afford PF-DBT as a black solid (0.17 g, 64%).

^{1}H NMR (500 MHz, $CDCl_3$): δ 8.10 (br, 2 H), 7.90 (br, 2 H), 7.71–7.60 (m, 2H), 7.53–7.13 (m, 10H, aromatic and vinylic), 1.92–2.08 (m, 4 H), 1.00–1.29 (m, 20 H), 0.81 (t, J = 6.5 Hz, 6 H), 0.60–0.76 (m, 4 H). Anal. calcd for $C_{47}H_{50}N_2S_3$: C, 76.38; H, 6.82; N, 3.79; S, 13.02. Found: C, 75.78; H, 7.25; N, 3.47; S, 12.84.

Measurements and characterization

^{1}H NMR spectra were recorded on a Bruker AVANCE 500-MHz spectrometer with *d*-chloroform as solvent and tetramethylsilane (TMS) as the internal standard. The elemental analysis was carried out with a Thermoquest CHNS-Ovelemental analyzer. The gel permeation chromatographic (GPC) analysis was carried out with a Waters 410 instrument with tetrahydrofuran as the eluent (flow rate: 1 mL min^{-1}, at 35 °C) and polystyrene as the standard. The thermogravimetric analysis (TGA) was performed on a Perkin Elmer Pyris 1 analyzer under nitrogen atmosphere (100 mL min^{-1}) at a heating rate of 10 °C min^{-1}. UV-visible absorption spectra were measured using a Shimadzu UV-3100 spectrophotometer. Electrochemical measurements of these derivatives were performed with a Bioanalytical Systems BAS 100 B/W electrochemical workstation. Atomic force microscopy (AFM) images of blend films were carried out using a Nanoscope IIIa Dimension 3100. Transmission electron microscopy (TEM) images of blend films were performed on a FEI Technai-G^2 transmission electron microscope operated at an acceleration voltage of 200 kV.

Photovoltaic device fabrication and characterization

The BHJ solar cells were fabricated with the active layer consisting of the copolymers (PF-TBT, and PF-DBT) : PCBM with varied blend ratios (1 : 1, 1 : 2, 1 : 3, 1 : 4 w/w), respectively. ITO glass was cleaned by detergent, acetone and boiled in H_2O_2. A 50 nm layer of poly(3,4-ethylene dioxythiophene) : poly(styrenesulfonate) (PEDOT : PSS)(Bayer PVP Al 4083) as a modified layer was spin-coated onto the pre-cleaned ITO glass substrate and then dried at 120 °C for 15 min on a hot plate. The copolymers were dissolved in chlorobenzene to make 4 mg ml^{-1} solutions, followed by blending with PCBM (purchased from Lumtec. Corp) in varied blend ratios (1 : 1, 1 : 2, 1 : 3, 1 : 4 w/w). The active layers were obtained by spin-coating the blend solutions and the thickness of films were ~70 nm, as measured with the Ambios Technology XP-2. Finally, the cathode of LiF (0.6 nm)/Al (100 nm) was thermally deposited to finish the device fabrication. The hole-only devices with a general structure of ITO/PEDOT : PSS/copolymer : PCBM(50 nm)/Au (60 nm) were fabricated for hole mobility measurements by space charge limited current (SCLC) method. The active area was about 5 mm^2. Current–voltage (*J*–*V*) characteristics were recorded using a Keithley 2400 Source Meter in the dark and under 100 mW cm^{-2} simulated AM 1.5 G irradiation (Sciencetech SS-0.5 K Solar Simulator). The spectral response was recorded by a SR830 lock-in amplifier under short circuit conditions when devices were illuminated with a monochromatic light from a Xeon lamp. All fabrication and characterizations were performed under ambient atmosphere at room temperature.

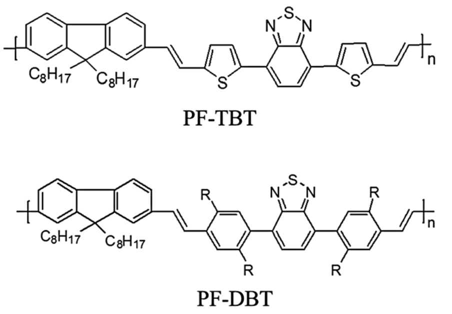

Scheme 1 Chemical structures of PF-TBT and PF-DBT.

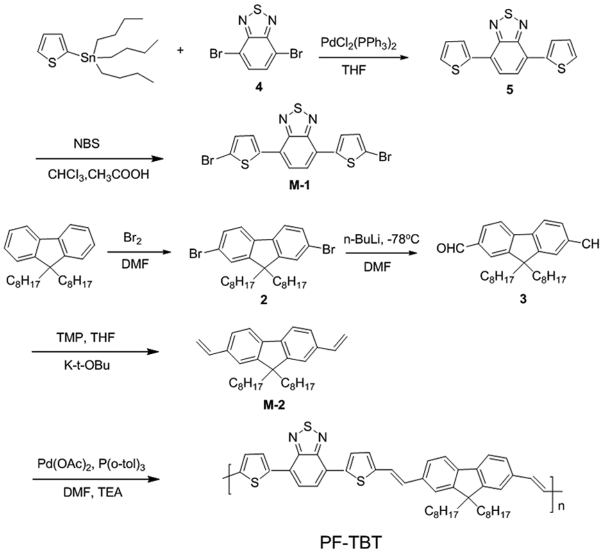

Scheme 2 Synthetic routes of the monomers and PF-TBT.

Results and discussion

Synthesis and characterization

The chemical structures of PF-TBT and PF-DBT are shown in Scheme 1. The PF group was bridged to the π-conjugated systems through the vinylene linkage. An octyl group was

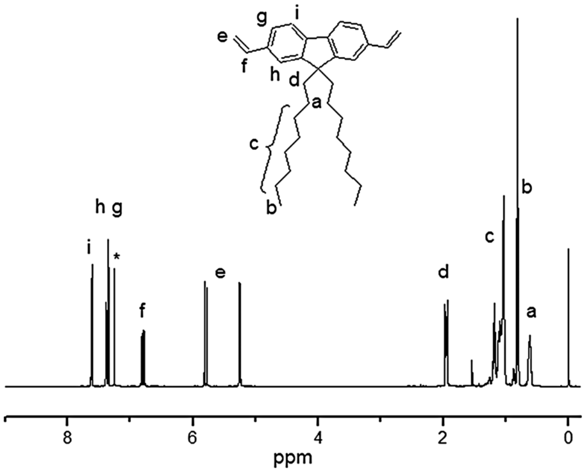

Fig. 1 The ^{1}H NMR spectrum and chemical structure of monomer (M-2) in $CDCl_3$ solution.

introduced onto the C_9 atom for the sake of solubility. PF-TBT was synthesized by Heck cross-coupling polymerization with the synthesis route shown in Scheme 2. 4,7-Bis(5-bromo-2-thienyl)-2,1,3-benzothiadiazole (M-1) was synthesized according to the procedures described in the literature.[33] 2,7-Diethenyl-9,9-di-*n*-octylfluorene (M-2) was synthesized in a multistep synthesis. The ^{1}H NMR spectrum of monomer M-2 in $CDCl_3$ is shown in Fig. 1. Starting from commercially available fluorene, in three steps 2,7-diformyl-9,9-di-*n*-octylfluorene was obtained. Similarly, 2,7-diethenyl-9,9-di-*n*-octylfluorene was synthesized by a modified procedure in high yield. In the conversion from aldehyde to vinylene, we added potassium *tert*-butoxide as strong base under room temperature conditions instead of *n*-BuLi at −40 °C, which can reach higher yields. Because fluorenevinylene is less stable and radical polymerization happens at room temperature under irradiation, **M-2** should be copolymerized quickly with **M-1** by Heck coupling reaction with $Pd(OAc)_2$ and $P(o\text{-tol})_3$ as catalysts and triethylamine as a base in DMF to obtain PF-TBT. The synthesized copolymer was highly soluble in common organic solvents such as chloroform, tetrahydrofuran, and chlorobenzene at room temperature.

Thermal properties

The thermal property of PF-TBT was evaluated by thermogravimetric analysis (TGA). The thermal property of PF-DBT was reported previously.[30] Fig. 2 shows the TGA curves of PF-TBT and PF-DBT at the heating rate of 10 °C min^{-1} under a nitrogen atmosphere. As shown in Fig. 2, the decomposition temperatures (T_d) of PF-TBT and PF-DBT were 402 °C and 389 °C, respectively, which suggests relatively high thermal stability. The high thermal stability of the resulting polymers prevents the deformation and degradation of the polymeric active layer under applied electric fields. Data on the polymerization results and thermal properties of PF-TBT and PF-DBT are listed in Table 1.

Table 1 Polymerization results and thermal properties of copolymers

Polymers	$M_w(10^4)$	$M_n(10^4)$	PDI	TGA (T_d)
PF-TBT	0.76	0.66	1.15	402
PF-DBT	12.2	6.25	1.95	389

Optical properties

The UV-vis absorption spectra of the PF-TBT in dilute chloroform solution (concentration 1×10^{-5} M) and thin film are shown in Fig. 3a. For comparison, those of PF-DBT in solution and film are also shown in Fig. 3a and the maximum absorptions are listed in Table 2. The absorption spectrum of PF-TBT in solution shows three peaks with the maximum absorption peaks located at 318, 400 and 536 nm. The shorter wavelength peak of PF-TBT in the region of 300–500 nm which is consistent with the absorption of PF-DBT, can be assigned to the absorption of a fluorine unit and π–π* transition of the conjugated polymer backbone, whereas the longer wavelength peak at 536 nm originates from the ICT interaction between the electron-donating fluorene unit and the electron-accepting benzothiadiazole unit.

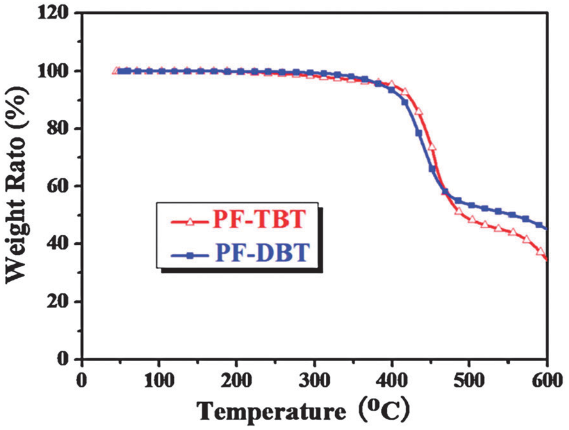

Fig. 2 TGA curves of the PF-TBT and PF-DBT at the heating rate of 10 °C min^{-1} under nitrogen atmosphere.

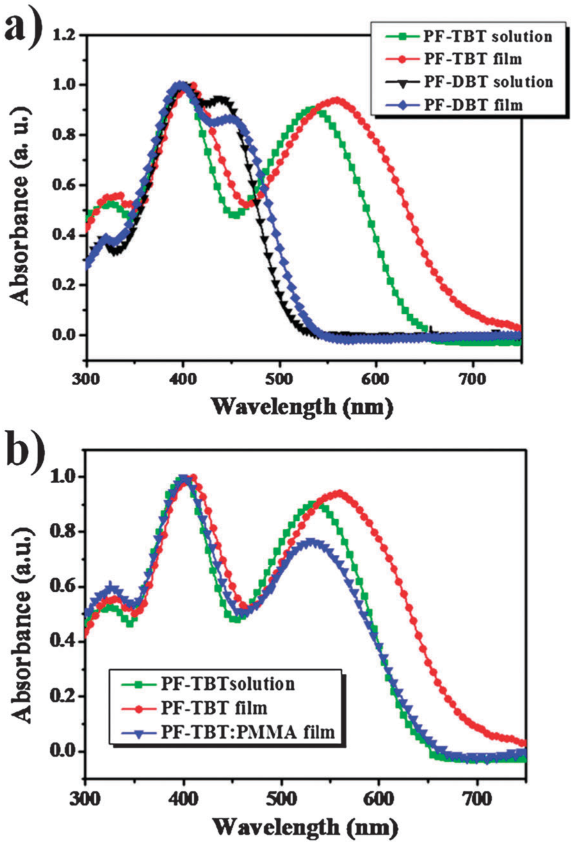

Fig. 3 Normalized UV-vis absorption: PF-TBT and PF-DBT in chloroform solution and film (a); PF-TBT in PMMA film, chloroform solution and film (b).

The optical absorption spectra of the copolymers in a thin film are generally similar in shape to that in dilute solution. Compared to its counterparts in dilute solution, the optical absorption of PF-TBT in a film exhibited red shift by *ca.* 24 nm, presumably indicating the formation of a π-stacked structure in the solid state that could facilitate harvesting of sunlight for photovoltaic applications.[30,34] In order to see whether π-stacking was the cause of the 24 nm red-shift in the absorption spectra, we prepared the film of PF-TBT

Table 2 Optical and electrochemical properties of PF-TBT and PF-DBT

Polymers	$\lambda_{max}^{abs,\ sol}$	$\lambda_{max}^{abs,\ film}$	E_g^{opt}	E_{ox}^{onset}	HOMO	E_{red}^{onset}	LUMO	E_g^{ec}
PF-DBT	400/436	400/449	2.32	0.71	−5.45	−1.69	−3.05	2.40
PF-TBT	400/536	409/560	1.82	0.64	−5.37	−1.32	−3.41	1.96

dispersed in PMMA (with a weight ratio of 1 : 100) and measured the absorption spectrum, shown in Fig. 3b, together with the absorption spectra of PF-TBT in solution and film. It can be seen that the absorption behavior of PF-TBT dispersed in PMMA is similar to that in solution. There is a 24 nm red shift of the absorption peak of pure PF-TBT film compared to that of the PF-TBT : PMMA film, which confirms that π-stacking causes the 24 nm red shift in the absorbance spectra of PF-TBT. From the low energetic edge of the absorption spectrum of the individual copolymer, the band gap of PF-DBT was estimated to be 2.32 eV (absorption edge: ~534 nm), while smaller band gaps of 1.82 eV were calculated for PF-TBT (absorption edge: ~680 nm), respectively, indicating the strong electron-donating conjugated bridge between the electron-donating unit and electron-accepting unit could lead to an enhanced ICT transition band, resulting in the extension of the absorption spectral range.

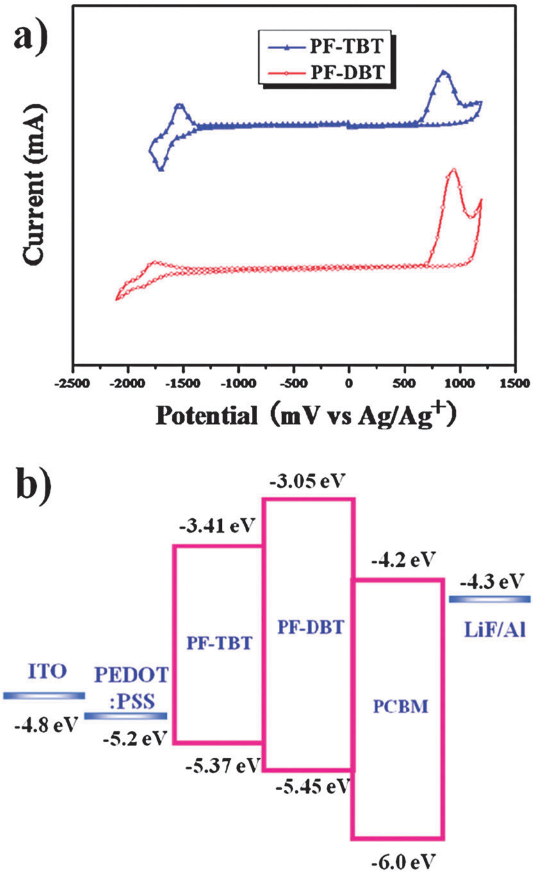

Fig. 4 (a) Cyclic voltammograms of the copolymer thin films on Pt wires in 0.1M TBAPF$_6$ in acetonitrile. The scan rates used were 30–50 mV s^{-1}; (b) energy level diagrams for PF-TBT, PF-DBT, and PCBM.

Electrochemical properties

Cyclic voltammetry of the copolymer films was performed in acetonitrile with 0.1 M tetrabutylammonium hexafluorophosphate (TBAPF$_6$) as the supporting electrolyte at scan rates of 30–50 mV s^{-1}. Platinum wire electrodes were used as both counter and working electrodes, and silver/silver ion (Ag in 0.1M AgNO$_3$ solution, from Bioanalytical Systems, Inc.) was used as the reference electrode. Ferrocene/ferrocenium (Fc/Fc$^+$) was used as the internal standard.

The redox curves of PF-TBT and that of PF-DBT are shown in Fig. 4a as a comparison. A complete picture of the band structure of the copolymers is presented in Fig. 4b. On the anodic sweep, two copolymers showed an irreversible oxidation with onset potentials of 0.71 V (*versus* Ag/Ag$^+$) for PF-DBT, and 0.64 V for PF-TBT, respectively. In contrast, the cathodic sweep showed onset reduction potentials of −1.69 V (*versus* Ag/Ag$^+$) for PF-DBT, and −1.32 V for PF-TBT.

From the onset oxidation potentials (E_{ox}^{onset}) and the onset reduction potentials (E_{red}^{onset}) of the polymers, HOMO and LUMO energy levels as well as the energy gap were calculated according to the following equations:[7,30]

$$\text{HOMO (eV)} = -\text{e}(E_{ox}^{onset} + 4.73)$$

$$\text{LUMO (ev)} = -\text{e}(E_{red}^{onset} + 4.73)$$

$$E_g^{ec}\ \text{(eV)} = \text{e}(E_{ox}^{onset} - E_{red}^{onset})$$

where E_{ox}^{onset} and E_{red}^{onset} are the measured onset potentials relative to Ag/Ag$^+$.

The results of the electrochemical measurements and calculated energy levels of the copolymers are listed in Table 2. From Table 2 we can see that the band gaps (E_g^{ec}) of PF-DBT and PF-TBT were estimated to be about 2.40 and 1.96, respectively, which are in good agreement with the optical band gap (E_g^{opt}). For the copolymer PF-TBT, the substitution of the stronger electron-donating conjugate bridge (thiophene unit) resulted in a lower LUMO level of −3.41 eV, a stable HOMO energy level of −5.37 eV and a lower E_g^{ec} compared with that of PF-DBT. The HOMO energy level of the donor polymer in a BHJ solar cell is very important for high device efficiency, as the V_{oc} of BHJ solar cell is determined by the difference between the HOMO level of the donor polymer and the LUMO of the acceptor. The relatively low HOMO level (−5.37 eV) of PF-TBT compared with polythiophene derivatives, such as P3HT (HOMO = −4.75 eV),[35] may be favored for the improvement of the V_{oc} when fabricating the BHJ solar cell with PF-TBT as the donor and PCBM as the acceptor. Besides the V_{oc}, J_{sc} is another key parameter to determine the efficiency of the solar cells. We know the J_{sc} is directly related with the absorption of the active layer. The broad absorption of the photon flux in the solar spectrum is the premise for high J_{sc}. The broad absorption means a narrow bandgap of the materials. We want a low-lying HOMO level for high V_{oc}. At the same time, we also want a narrow bandgap for high J_{sc}. Therefore the LUMO level of the material should also go towards a lower-lying position accordingly.[36] However, to guarantee the efficient electron transfer from the donor material to PCBM, the energy level cannot be too low. At least 0.3 eV over the LUMO level of PCBM (−4.2 eV) is required.[4] Here, PF-TBT with a LUMO level of −3.41 eV. The bandgap is 1.96 eV. Comparing with PF-DBT, PF-TBT has a lower-lying LUMO level and narrower bandgap (Fig. 4b) and accordingly a high J_{sc} for the solar cells based on PF-TBT is expected.

Photovoltaic properties

We fabricated BHJ solar cells with the structure of ITO/PEDOT : PSS/copolymer : PCBM/LiF/Al using the copolymer PF-TBT as the electron donor and PCBM as the electron acceptor. For comparison, BHJ solar cells based on PF-DBT with the same structure were also fabricated. We tried different compositions of the copolymer : PCBM (1 : 1, 1 : 2, 1 : 3, 1 : 4, w/w) to optimize the device performance. Fig. 5 shows the current–voltage (*J–V*) characteristics of the solar cells based on the two copolymers blended with PCBM and the photovoltaic data are summarized in Table 3. The solar cell based on PF-TBT : PCBM exhibited a V_{oc} of 0.86 V, J_{sc} of 3.97 mA cm^{-2}, FF of 0.35 and a PCE of 1.18%, while the cell based on PF-DBT : PCBM exhibited a V_{oc} of 1.04 V, J_{sc} of 3.23 mA cm^{-2}, FF of 0.48 and PCE of 1.64% under one sun of AM 1.5 solar simulator illumination (100 mW cm^{-2}).

The higher V_{oc} of the device based on PF-DBT : PCBM is due to the lower lying HOMO energy level (−5.45 eV) than that of PF-TBT (−5.37 eV), because V_{oc} is related to the difference between the LUMO energy level of the acceptor and the HOMO energy level of the donor within the active layer.

The higher J_{sc} of the device based on PF-TBT : PCBM than that of the device based on PF-DBT:PCBM could be explained by the broader absorption and lower band gap of PF-TBT, which is consistent with the broader external quantum efficiency (EQE) spectra (shown in Fig. 6) of the devices based on PF-TBT : PCBM.

As for FF, the devices based on PF-DBT : PCBM exhibited higher FF than the devices based on PF-TBT : PCBM. The FF of the solar cells is strongly influenced by the mobility and the surface morphology of the active layer.[37] We analysed the hole mobility of the polymer : PCBM composite films through the space charge limited current (SCLC) method.[38,39] The hole-only devices with a structure of ITO/PEDOT : PSS/copolymer : PCBM/Au were fabricated. Fig. 7 shows the *J–V* characteristics of the hole-only devices based on PF-TBT : PCBM and PF-DBT : PCBM with varied composition and the corresponding hole motilities are listed in Table 2. As the concentration of PCBM increased, the hole mobility of polymer : PCBM was enhanced. The hole mobility of the PF-DBT : PCBM (1 : 4, w/w) blend is 8.0 × 10^{-6} cm^2 V^{-1} S^{-1}, which is about 2.5 times of that of the PF-TBT : PCBM (1 : 4, w/w, 3.05 × 10^{-6} cm^2 V^{-1} S^{-1}) blend. The higher hole mobility of PF-DBT:PCBM blend might contribute to a more

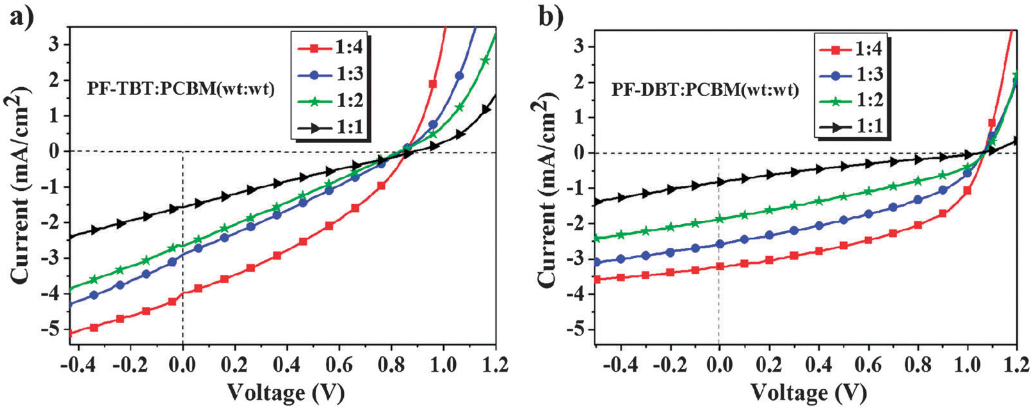

Fig. 5 *J–V* curves of the devices based on PF-TBT : PCBM (a) and PF-DBT : PCBM (b) with different blend ratios (1 :1, 1 :2, 1 : 3, 1 : 4, w/w) under the illumination of AM 1.5, 100 mW cm^{-2}.

Table 3 Photovoltaic performance of the solar cells based on PF-TBT : PCBM and PF-DBT : PCBM

Donor (polymer)	Blend ratio (D : A)	V_{oc}/V	J_{sc}/mA cm^{-2}	FF	PCE (%)	Hole mobility/cm^2 V^{-1} S^{-1}
PF-TBT	1 : 1	0.88	1.57	0.24	0.33	3.82 × 10^{-7}
PF-TBT	1 : 2	0.84	2.66	0.26	0.57	5.38 × 10^{-7}
PF-TBT	1 : 3	0.84	2.90	0.27	0.67	1.07 × 10^{-6}
PF-TBT	1 : 4	0.86	3.97	0.35	1.18	3.05 × 10^{-6}
PF-DBT	1 : 1	1.06	0.82	0.21	0.19	4.02 × 10^{-7}
PF-DBT	1 : 2	1.06	1.88	0.33	0.66	1.06 × 10^{-6}
PF-DBT	1 : 3	1.06	2.58	0.40	1.09	2.89 × 10^{-6}
PF-DBT	1 : 4	1.04	3.23	0.48	1.64	8.0 × 10^{-6}

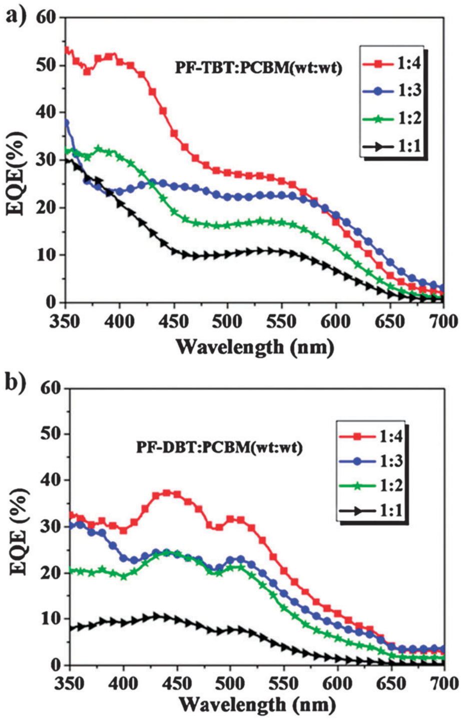

Fig. 6 The external quantum efficiency (EQE) based on PF-TBT : PCBM (a) and PF-DBT : PCBM (b) with different blend ratios (1 : 1, 1 : 2, 1 : 3, 1 : 4, w/w).

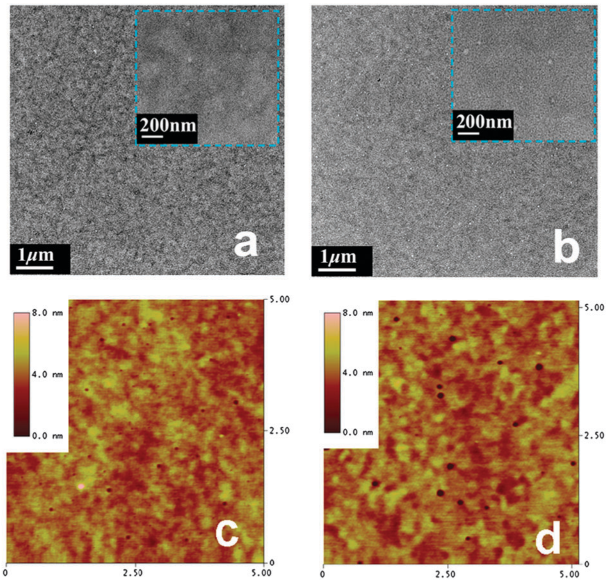

Fig. 8 TEM images and AFM topography images (5 μm × 5 μm) of PF-DBT : PCBM (a, c) and PF-TBT : PCBM (b, d) in 1 : 4 w/w blend ratio cast from chlorobenzene solutions.

balanced charge transport in the PF-DBT : PCBM composite layer and a more efficient carrier collection at the interface between the active layer and the respective electrode.[37,40]

In order to investigate the reason for the different FF of the cells based on PF-TBT : PCBM and on PF-DBT:PCBM, we also analyzed the surface morphology of PF-TBT : PCBM and PF-DBT : PCBM composite films (1 : 4, w/w) using atom force microscopy (AFM) and transmission electron microscopy (TEM). In the TEM image, the dark areas are attributed to PCBM domains because the electron scattering density of PCBM is higher than that of conjugated polymers.[41] The AFM and TEM images (Fig. 8) reveal a smooth surface with a root mean square (RMS) of 0.462 nm and the formation of more homogeneous morphology without obvious PCBM-rich domains in the PF-TBT : PCBM blend film. However the image of the PF-DBT : PCBM film becomes relatively rough with a RMS of 0.63 nm and significant phase separation with the formation of large PCBM-rich domains appearing. The PCBM-rich domains could improve the charge transportation and carrier collection effectively, which results in a reduction of recombination loses and an increase of FF.[40,42]

So, the higher hole mobility and the rough morphology with obvious phase separation of PF-DBT : PCBM blends could be the reason why the FF of the cell based on PF-TBT : PCBM was lower than that of the cells based on PF-DBT : PCBM.

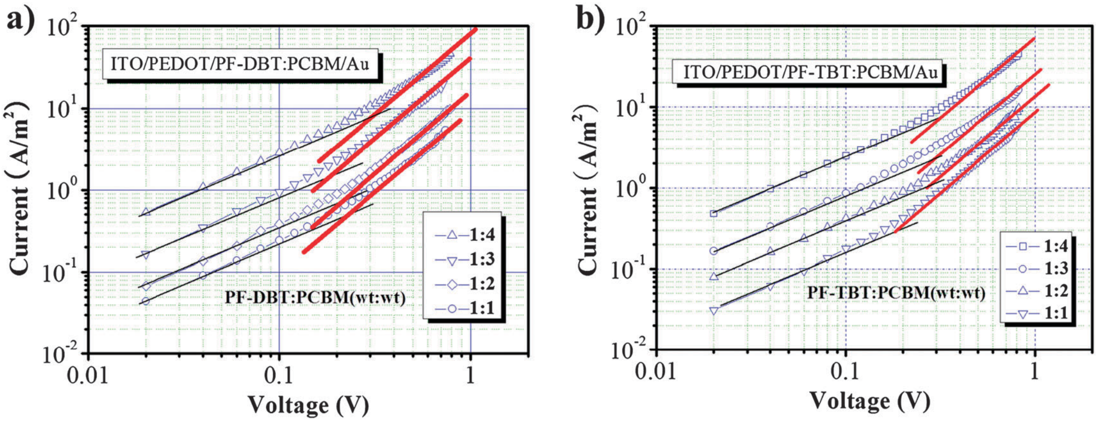

Fig. 7 *J–V* curve in the dark of an ITO/PEDOT/PF-TBT (PF-DBT) : PCBM/Au device in log axis for estimating the hole mobility of PF-DBT : PCBM (a) and PF-TBT : PCBM (b). The thickness of PF-TBT : PCBM and PF-DBT : PCBM are around 50 nm. The open rectangle symbols are the experimental data. The solid line from 0.01 to 0.25 V means log$J$ is fitted linearly dependent on log$V$ with a slope of 1. The solid line from 0.25 to 0.8 V log$J$ is fitted linearly dependent on log$V$ with a slope of 2 (SCLC area).

The PCE of a solar cell is determined by the open circuit voltage, the short circuit current density and the fill factor. We found that the solar cells based on PF-TBT : PCBM exhibited a V_{oc} of 0.86 V, J_{sc} of 3.97 mA cm^{-2}, FF of 0.35 and PCE of 1.18%, while a V_{oc} of 1.04 V, J_{sc} of 3.23 mA cm^{-2}, FF of 0.48 and PCE of 1.64% were found for the cell based on PF-DBT : PCBM under one sun of AM 1.5 solar simulator illumination (100 mW cm^{-2}). As compared to PF-DBT, the low band gap of PF-TBT is more desirable as a photovoltaic material and exhibited higher J_{sc} under illumination, but its lower mobility, smooth morphology without obvious phase separation and higher-lying HOMO level lead to a lower FF and V_{oc} in the devices based on PF-TBT : PCBM. Accordingly, the devices based on PF-DBT : PCBM composite films exhibited higher device performance than the devices based on PF-TBT : PCBM composite films.

Conclusions

In this work, we have successfully synthesized a novel polyfluorene (PF)-based low band gap copolymer PF-TBT by Heck cross-coupling polymerization. The introduction of a thiophene unit as a conjugated bridge between the electron-donating fluorene unit and electron-accepting 2,1,3-benzothiadiazole unit makes PF-TBT exhibit a broad absorption with an absorption edge close to 700 nm and an optical band gap of 1.82 eV. It is known that P3HT has a HOMO energy level of around 5.0 eV and the solar cells based on P3HT : PCBM show a V_{oc} of 0.6 V. Comparing with P3HT, the new material of PF-TBT has a lower-lying HOMO energy level of −5.37 eV and shows a higher V_{oc} of 0.86 V for solar cells. The bulk heterojunction (BHJ) solar cells using PF-TBT as donor and PCBM as acceptor exhibited a high V_{oc} of 0.86 V, and PCE of 1.18%. Although the power conversion efficiencies for the new copolymer are still not sufficiently high, this work provides a concept for developing D–A conjugated copolymers for photovoltaic applications.

Acknowledgements

This work was supported by the State Key Development Program for Basic Research of China (Grant No. 2009CB623605), the National Natural Science Foundation of China (Grant No. 20874035), Program for New Century Excellent Talents in Universities of China Ministry of Education, the 111 Project (Grant No. B06009), and the Project of Jilin Province (20080305).

Notes and references

1 (*a*) N. S. Sariciftci, L. Smilowitz, A. J. Heeger and F. Wudl, *Science*, 1992, **258**, 1474; (*b*) G. Yu, J. Gao, J. C. Hummelen, F. Wudl and A. J. Heeger, *Science*, 1995, **270**, 1789.
2 P. W. M. Blom, V. D. Mihailetchi, L. J. A. Koster and D. E. Markov, *Adv. Mater.*, 2007, **19**, 1551.
3 S. Günes, H. Neugebauer and N. S. Sariciftci, *Chem. Rev.*, 2007, **107**, 1324.
4 B. C. Thompson and J. M. J. Fréchet, *Angew. Chem., Int. Ed.*, 2008, **47**, 58.
5 H. Y. Chen, J. H. Hou, S. Q. Zhang, Y. Y. Liang, G. W. Yang, Y. Yang, L. P. Yu, Y. Wu and G. Li, *Nat. Photonics*, 2009, **3**, 649.
6 P. F. Xia, J. P. Lu, C. H. Kwok, H. Fukutani, M. S. Wong and Y. Tao, *J. Polym. Sci., Part A: Polym. Chem.*, 2009, **47**, 137.
7 S. P. Wen, J. N. Pei, Y. H. Zhou, L. L. Xue, B. Xu, Y. W. Li and W. J. Tian, *J. Polym. Sci., Part A: Polym. Chem.*, 2009, **47**, 1003.
8 J. Y. Kim, K. Lee, N. E. Coates, D. Moses, T. Q. Nguyen, M. Dante and A. J. Heeger, *Science*, 2007, **317**, 222.
9 H.-L. Yip, S. K. Hau, N. S. Baek, H. Ma and A. K.-Y. Jen, *Adv. Mater.*, 2008, **20**, 2376.
10 Q. Q. Qiao and J. T. Mcleskey, *Appl. Phys. Lett.*, 2005, **86**, 153501.
11 Y. W. Li, L. L. Xue, H. J. Xia, B. Xu, S. P. Wen and W. J. Tian, *J. Polym. Sci., Part A: Polym. Chem.*, 2008, **46**, 3970.
12 (*a*) N. Blouin, A. Michaud, D. Gendron, S. Wakim, E. Blair, R. Neagu-Plesu, M. Belletete, G. Durocher, Y. Tao and M. Leclerc, *J. Am. Chem. Soc.*, 2008, **130**, 732; (*b*) K. P. Li, J. L. Qu, B. Xu, Y. H. Zhou, L. J. Liu, P. Peng and W. J. Tian, *New J. Chem.*, 2009, **33**, 2120.
13 M. M. Wienk, M. Turbiez, J. Gilot and R. A. J. Janssen, *Adv. Mater.*, 2008, **20**, 2556.
14 F. Huang, K.-S. Chen, H.-L. Yip, S. K. Hau, O. Acton, Y. Zhang, J. D. Luo and A. K-Y. Jen, *J. Am. Chem. Soc.*, 2009, **131**, 13886.
15 J. H. Hou, H. Y. Chen, S. Q. Zhang, G. Li and Y. Yang, *J. Am. Chem. Soc.*, 2008, **130**, 16144.
16 R. P. Qin, W. W. Li, C. H. Li, C. Du, C. Veit, H. Schleiermacher, M. Andersson, Z. S. Bo, Z. P. Liu, O. Inganas, U. Wuerfel and F. L. Zhang, *J. Am. Chem. Soc.*, 2009, **131**, 14612.
17 (*a*) K. Colladet, S. Fourier, T. J. Cleij, L. Lutsen, J. Gelan, D. Vanderzande, L. H. Nguyen, H. Neugebauer, N. S. Sariciftci, A. Aguirre, G. Janssen and E. Goovaerts, *Macromolecules*, 2007, **40**, 65; (*b*) S. M. Zhang, H. J. Fan, Y. Liu, G. J. Zhao, Q. K. Li, Y. F. Li and X. W. Zhan, *J. Polym. Sci., Part A: Polym. Chem.*, 2009, **47**, 2843.
18 S. Wakim, S. Beaupre, N. Blouin, B.-R. Aich, S. Rodman, R. Gaudiana, Y. Tao and M. Leclerc, *J. Mater. Chem.*, 2009, **19**, 5351.
19 G. Y. Sang, Y. P. Zou and Y. F. Li, *J. Phys. Chem. C*, 2008, **112**, 12058.
20 C. J. Brabec, C. Winder, N. S. Saraciftci, J. C. Hummelen, A. Dhanabalan, P. A. Van Hall and R. A. J. Jassen, *Adv. Funct. Mater.*, 2002, **12**, 709.
21 N. Blouin, A. Michaud and M. Leclerc, *Adv. Mater.*, 2007, **19**, 2295.
22 N. Leclerc, A. Michaud, K. Sirois, J.-F. Morin and M. Leclerc, *Adv. Funct. Mater.*, 2006, **16**, 1694.
23 A. K. Agrawal and S. A. Jenekhe, *Chem. Mater.*, 1996, **8**, 579.
24 Y. Cui, X. Zhang and S. A. Jenekhe, *Macromolecules*, 1999, **32**, 3824.
25 T. Yasuda, Y. Sakai, S. Aramaki and T. Yamamoto, *Chem. Mater.*, 2005, **17**, 6060.
26 U. Scherf and E. J. W. List, *Adv. Mater.*, 2002, **14**, 477.
27 B. Liu, W. L. Yu, Y. H. Lai and W. Huang, *Chem. Mater.*, 2001, **13**, 1984.
28 Y.-J. Cheng, S.-H. Yang and C.-S. Hsu, *Chem. Rev.*, 2009, **109**, 5868.
29 M. Svensson, F. L. Zhang, S. C. Veenstra, W. J. H. Verhees, J. C. Hummelen, J. M. Kroon, O. Inganäs and M. R. Andersson, *Adv. Mater.*, 2003, **15**, 988.
30 S. P. Wen, J. N. Pei, Y. H. Zhou, P. F. Li, L. L. Xue, Y. W. Li, B. Xu and W. J. Tian, *Macromolecules*, 2009, **42**, 4977.
31 P. Anuragudom, S. S. Newaz, S. Phanichphant and T. R. Lee, *Macromolecules*, 2006, **39**, 3494.
32 K. Pilgram, M. Zupan and R. Skile, *J. Heterocycl. Chem.*, 1970, **7**, 629.
33 C. J. Shi, Y. Wu, W. J. Zeng, Y. Q. Xie, K. X. Yang and Y. Cao, *Macromol. Chem. Phys.*, 2005, **206**, 1114.
34 Q. Peng, K. Park, T. Lin, M. Durstock and L. M. Dai, *J. Phys. Chem. B*, 2008, **112**, 2801.

35 C. J. Shi, Y. Yao, Y. Yang and Q. B. Pei, *J. Am. Chem. Soc.*, 2006, **128**, 8980.

36 M. C. Scharber, D. Wuhlbacher, M. Koppe, P. Denk, C. Waldauf, A. J. Heeger and C. L. Brabec, *Adv. Mater.*, 2006, **18**, 789.

37 J. K. J. Van Duren, X. Yang, J. Loos, C. W. T. Bulle-Lieuwma, A. B. Sieval, J. C. Hummelen and R. A. J. Janssen, *Adv. Funct. Mater.*, 2004, **14**, 425.

38 P. W. M. Blom, M. J. M. DeJong and M. G. VanMunster, *Phys. Rev. B: Condens. Matter*, 1997, **55**, R656.

39 Y. H. Zhou, J. N. Pei, Q. F. Dong, X. B. Sun, Y. Q. Liu and W. J. Tian, *J. Phys. Chem. C*, 2009, **113**, 7882.

40 Gadisa, F. L. Zhang, D. Sharma, M. Svensson, M. R. Andersson and O. Inganäs, *Thin Solid Films*, 2007, **515**, 3126.

41 T. Martens, J. D'Haen, T. Munters, Z. Beelen, L. Goris, J. Manca, M. D'Olieslaeger, D. Vanderzande, L. De Schepper and R. Andriessen, *Synth. Met.*, 2003, **138**, 243.

42 R. Demadrille, N. Delbosc, Y. Kervella, M. Firon, R. D. Bettignies, M. Billon, P. Rannou and A. Pron, *J. Mater. Chem.*, 2007, **17**, 4661.